Detection of Near-Atmospheric Concentrations of CO 2 by an Olfactory Subsystem in the Mouse

Ji Hu, *et al.*

Science **317**, 953 (2007);
DOI: 10.1126/science.1144233

Science (print ISSN 0036-8075; online ISSN 1095-9203) is published weekly, except the last week in December, by the American Association for the Advancement of Science, 1200 New York Avenue NW, Washington, DC 20005.

reports that the IC is critical for consolidation, storage, and extinction of CTA (*7*, *13*, *21*, *22*). Although the map of CS-UCS association sites in CTA encoding is still incomplete and probably includes subcortical structures (*23*), once the association is formed, the IC is likely to store elements of the associative hedonic or incentive value of the CS (*24*). In contrast, whereas the IC is documented to detect taste novelty that facilitates encoding of CTA (*4*, *7*, *13*, *14*, *21*), the present data are in line with the possibility that taste familiarity per se is not stored in the IC.

So far, we have found no evidence that the effect of ZIP on associative taste memory in cortex is reversible; hence, we heuristically propose that the PKMζ inhibitor might practically erase some long-term memory associations. We are aware of the difficulties in concluding that a memory trace is erased from the lack of ability to detect a change in performance that is attributed to that trace. This inherent difficulty haunts the long-standing debate on whether amnesia is a storage or a retrieval deficit, yet does not preclude the assumption that amnesia is a storage deficit (*8*, *9*, *25*).

Recent data on reactivation-dependent vulnerability of memory to amnesic agents (*8*, *9*) reemphasize the frailty of the engram—an attribute long recognized by cognitive psychologists (*26*), but somehow mostly ignored till recently by neuroscientists. Our data reinforce the notion that memory traces are prone to swift interferences long after their encoding. In contrast to these earlier studies, however, no reactivation is needed to render the trace susceptible to ZIP. The possibility that the trace reactivates implicitly is low given that classical amnesic agents, e.g., macromolecular synthesis inhibitors, have no effect on the long-term CTA trace that has not been reactivated (*7*, *13*).

The possibility cannot yet be excluded that vulnerability of memory to PKMζ inhibition in cortex might wane. If so, then the temporal window of "cellular consolidation," i.e., the stabilization process that is postulated to occur in synapses and cell bodies after memory encoding (*8*), lingers far longer than originally thought. This conclusion is even more striking given that elemental CTA seems hippocampus-independent, excluding a "systems consolidation" process in which the hippocampal trace invades neocortex over days to weeks (*8*). An alternative possibility is that PKMζ permanently maintains long-term memory and, thus, is a target for amnesic agents as long as the memory persists. In this case, defining consolidation on the basis of vulnerability to amnesic agents (*8*) requires reconsideration.

How does PKMζ inhibition disrupt memory in neocortex? If work on LTP in the hippocampus is a guide, the effect of PKMζ might be on the microstructure of preexisting synapses, resulting in a doubling of the number of functional postsynaptic AMPA-type glutamate receptors (*27*). Our results indicate, however, that these changes, even weeks after learning, are not indelible modifications of synaptic structure, but remain dependent on ongoing enzymatic activity and, thus, are capable of rapid and dynamic alterations by experimental manipulation or, perhaps, in the course of incorporation of new experience into associative knowledge schemas in cortex (*28*). The idea that persistent enzymatic activity keeps memory going has been raised on the basis of theoretical considerations (*29*–*31*). The finding that this takes place, via PKMζ, not only in LTP and hippocampus (*1*, *6*, *27*), but also in long-term memory in neocortex, has, in addition to theoretical implications, potential clinical significance, e.g., in the field of cognitive enhancement.

References and Notes

1. E. Pastalkova *et al.*, *Science* **313**, 1141 (2006).
2. L. R. Squire, P. J. Bayley, *Curr. Opin. Neurobiol.* **17**, 185 (2007).
3. Y. Dudai, *Memory from A to Z: Keywords, Concepts, and Beyond* (Oxford Univ. Press, Oxford, 2002).
4. A. Bahar, Y. Dudai, E. Ahissar, *J. Neurophysiol.* **92**, 3298 (2004).
5. Materials and methods are described in supporting material on *Science* Online.
6. D. S. F. Ling *et al.*, *Nat. Neurosci.* **5**, 295 (2002).
7. K. Rosenblum, N. Meiri, Y. Dudai, *Behav. Neur. Biol.* **59**, 49 (1993).
8. Y. Dudai, *Annu. Rev. Psychol.* **55**, 51 (2004).
9. K. Nader, *Trends Neurosci.* **26**, 65 (2003).
10. Y. Dudai, M. Eisenberg, *Neuron* **44**, 93 (2004).
11. N. C. Tronson, S. L. Wiseman, P. Olausson, J. R. Taylor, *Nat. Neurosci.* **9**, 167 (2006).
12. X. Dugas du Villard, C. Her, P. MacLeod, *Chem. Senses* **6**, 143 (1981).
13. D. E. Berman, S. Hazvi, K. Rosenblum, R. Seger, Y. Dudai, *J. Neurosci.* **18**, 10037 (1998).
14. F. Bermudez-Rattoni, *Nat. Rev. Neurosci.* **5**, 209 (2004).
15. M. T. Koh, E. E. Wilkins, I. L. Bernstein, *Behav. Neurosci.* **117**, 1416 (2003).
16. C. Roman, N. Nebieridze, A. Sastre, S. Reilly, *Behav. Neurosci.* **120**, 1257 (2006).
17. K. Rosenblum, D. E. Berman, S. Hazvi, R. Lamprecht, Y. Dudai, *J. Neurosci.* **17**, 5129 (1997).
18. O. Buresova, J. Bures, *Behav. Brain Res.* **1**, 299 (1980).
19. K. Yefet *et al.*, *Eur. J. Neurosci.* **24**, 1434 (2006).
20. M. E. Stone, B. S. Grimes, D. B. Katz, *Learn. Mem.* **12**, 579 (2005).
21. D. E. Berman, Y. Dudai, *Science* **291**, 2417 (2001).
22. M. Eisenberg, T. Kobilo, D. E. Berman, Y. Dudai, *Science* **301**, 1102 (2003).
23. T. Yamamoto, T. Shimura, N. Sako, Y. Yasoshima, N. Sakai, *Behav. Brain Res.* **65**, 123 (1994).
24. B. W. Balleine, A. Dickinson, *J. Neurosci.* **20**, 8954 (2000).
25. K. Nader, S. H. Wang, *Learn. Mem.* **13**, 530 (2006).
26. E. C. Bartlett, *Remembering: A Study in Experimental and Social Psychology* (Cambridge Univ. Press, Cambridge, 1932).
27. D. S. F. Ling, L. S. Benardo, T. C. Sacktor, *Hippocampus* **16**, 443 (2006).
28. D. Tse *et al.*, *Science* **316**, 76 (2007).
29. F. Crick, *Nature* **312**, 101 (1984).
30. J. D. Buxbaum, Y. Dudai, *J. Biol. Chem.* **264**, 9344 (1989).
31. P. Miller, A. M. Zhabotinsky, J. E. Lisman, X. J. Wang, *PLoS Biol.* **3**, e107 (2005).

32. The support of the Israeli Science Foundation (ISF), Jerusalem, to Y.D. is gratefully acknowledged. T.C.S. is supported by NIH R01 MH53576 and MH57068.

Supporting Online Material

www.sciencemag.org/cgi/content/full/317/5840/951/DC1
Materials and Methods
Fig. S1
References

26 April 2007; accepted 6 July 2007
10.1126/science.1144334

Detection of Near-Atmospheric Concentrations of CO_2 by an Olfactory Subsystem in the Mouse

Ji Hu,[1,2]* Chun Zhong,[1,2]* Cheng Ding,[1] Qiuyi Chi,[3] Andreas Walz,[4] Peter Mombaerts,[4] Hiroaki Matsunami,[3] Minmin Luo[1]†

Carbon dioxide (CO_2) is an important environmental cue for many organisms but is odorless to humans. It remains unclear whether the mammalian olfactory system can detect CO_2 at concentrations around the average atmospheric level (0.038%). We demonstrated the expression of carbonic anhydrase type II (CAII), an enzyme that catabolizes CO_2, in a subset of mouse olfactory neurons that express guanylyl cyclase D (GC-D$^+$ neurons) and project axons to necklace glomeruli in the olfactory bulb. Exposure to CO_2 activated these GC-D$^+$ neurons, and exposure of a mouse to CO_2 activated bulbar neurons associated with necklace glomeruli. Behavioral tests revealed CO_2 detection thresholds of ~0.066%, and this sensitive CO_2 detection required CAII activity. We conclude that mice detect CO_2 at near-atmospheric concentrations through the olfactory subsystem of GC-D$^+$ neurons.

CO_2 is an olfactory stimulus for many invertebrates (*1*, *2*). CO_2 levels fluctuate locally with biological activities, such as animal respiration, plant photosynthesis, and the decomposition of organic matter. CO_2 signals regulate many insect innate behaviors, such as seeking food and hosts, avoiding stressful environments, and ovipositioning (*3*–*6*). CO_2 has no discernable odor to humans, but at high concentrations (>30%), it produces a pungent trigeminal sensation in the nasopharynx (*7*). Carbonic anhydrase (CA), an enzyme that is implicated in CO_2 sensing by peripheral systems such as carotid chemoreceptors (*2*, *8*), is expressed in a subset of olfactory sensory neurons (OSNs) in several vertebrate species (*8*, *9*). Studies indicate that rats can detect CO_2 at levels above 0.5% (*10*, *11*). It remains unknown whether mammals can detect

CO_2 at concentrations near the atmospheric level (0.038%), and if so, whether this detection is mediated by a specialized olfactory subsystem.

In the mouse olfactory epithelium (OE), conventional OSNs use adenosine 3′-5′ monophosphate (cAMP) in odorant-evoked signal transduction, but a minor population of neurons appears to use guanosine 3′-5′ monophosphate (cGMP) (*12*–*14*). Unlike conventional OSNs, this minor population of cells expresses phosphodiesterase 2A (PDE2A), guanylyl cyclase D (GC-D), and cGMP-sensitive cyclic nucleotide-gated (CNG) channels (*12*–*14*). They project axons to the necklace glomeruli, a set of glomeruli that form a "necklace" in the caudal end of the olfactory bulb (OB) (*13*, *15*). The necklace glomeruli have been implicated in detecting suckling pheromones and pheromonal compounds (*16*, *17*). Here we show that mice can sense CO_2 at near-atmospheric levels through the subset of olfactory neurons that express PDE2A and GC-D.

We first examined the gene expression profile of neurons expressing PDE2A ($PDE2A^+$ neurons) by single-cell serial analysis of gene expression of dissociated cells from the caudal OE of mice (*18*). We found that $PDE2A^+$ neurons expressed high levels of CA type II (CAII), whereas conventional OSNs did not (fig. S1, A to C). Expression of *CAII/Car2* mRNA by a subset of OE cells was verified by in situ hybridization (fig. S1D). Immunostaining showed abundant CAII expression by a small population of cells in the caudal OE. Most of these $CAII^+$ cells clustered with bilateral symmetry in the cul-de-sac regions within the caudal recesses of the nasal cavity (Fig. 1A). CAII localized with PDE2A in the OE (Fig. 1, B to D) and in ~20 glomeruli more than 30 μm in diameter in the caudal OB (Fig. 1, E to H; and fig. S2, $n = 6$ mice). Because PDE2A in turn is coexpressed with GC-D (*13*, *14*), we analyzed a mouse strain with a targeted mutation in the *GC-D* locus that produces bicistronic messages causing cotranslation of GC-D with a fusion protein of tau and green fluorescent protein (GFP) (GCD-ITG mice). CAII immunoreactivity and GFP intrinsic fluorescence completely overlapped in the OE (Fig. 1, I to K) and OB (Fig. 1, L to N, $n = 2$ mice). Henceforth, we refer to the subset of $CAII^+$–$PDE2A^+$–$GC\text{-}D^+$ neurons as $GC\text{-}D^+$ neurons.

CA catalyzes the reversible reaction of $CO_2 + H_2O \rightleftharpoons HCO_3^- + H^+$ (*19*, *20*). Because CA is implicated in CO_2 sensing, we tested whether $GC\text{-}D^+$ neurons respond to CO_2 using calcium imaging in an intact OE preparation from GCD-ITG mice (*18*, *21*). OSNs were incubated with rhod-2 acetoxymethyl ester (AM), a calcium-sensitive red fluorescent dye. $GC\text{-}D^+$ neurons were identified by intrinsic green fluorescence of GFP in their dendritic knobs and somata (Fig. 2A), and the uptake of rhod-2 AM dye was confirmed by red fluorescence (Fig. 2B). Tissue was continuously superfused with oxygenated HEPES-based Ringer solution. CO_2 was delivered by superfusing CO_2-bubbled Ringer solution into the imaging chamber, resulting in peak CO_2 concentrations of 0.4 to 6.4 mM as calculated by CO_2 solubility (*22*). After CO_2 application, we observed fluorescence enhancement in both dendritic knobs and underlying somata of $GC\text{-}D^+$ neurons (Fig. 2C, $n = 428$ cells). CO_2 responses of $GC\text{-}D^+$ neurons were dose-dependent, with substantial activation starting at 1.0 mM CO_2 (Fig. 2D). $GC\text{-}D^+$ neurons were not activated by CO_2-free Ringer solution with adjusted pH or bicarbonate levels (Fig. 2E and fig. S3A). When tested with 6.4 mM CO_2, most $GC\text{-}D^-$ cells were not activated [$n = 256$ out of 260 (256/260) tested], and a few of them were only weakly activated (fig. S4, $n = 4/260$).

To examine the role of CA in CO_2 sensing by $GC\text{-}D^+$ neurons, we applied acetazolamide (AZ, 1 mM), a CA enzymatic inhibitor. AZ completely eliminated the CO_2 responses (Fig. 2F and fig. S3B). Calcium signals in response to CO_2 were absent in Ca^{2+}-free Ringer solution, indicating that calcium signals were due to external calcium influx (Fig. 2G and fig. S3C). Low concentrations of L-*cis*-diltiazem (10 μM), a CNG channel blocker (*23*), reversibly blocked the response of $GC\text{-}D^+$ neurons to CO_2 (Fig. 2, H and I). Thus, CO_2 specifically activates $GC\text{-}D^+$ neurons, and this activation requires CA enzymatic activity and the opening of CNG channels.

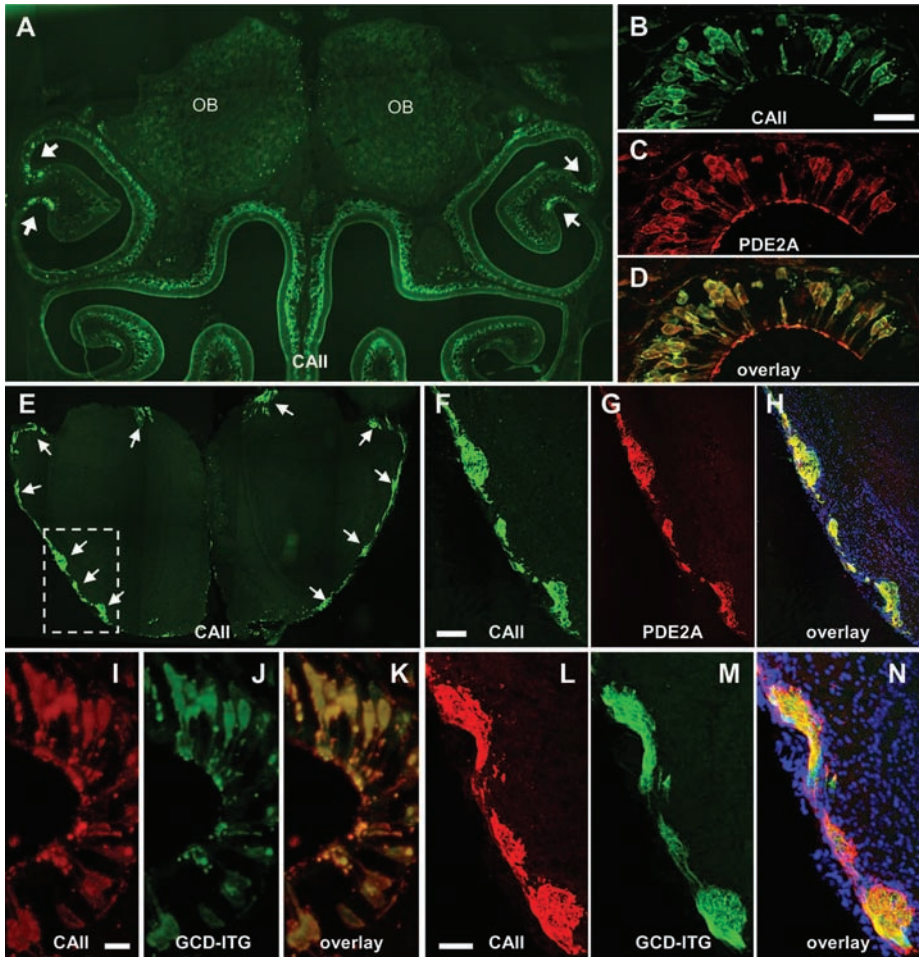

Fig. 1. CAII immunoreactivity in $GC\text{-}D^+$ neurons and necklace glomeruli. **(A)** Bilaterally symmetric distribution of $CAII^+$ cells (arrows) in the OE. **(B)** High-power view of CAII immunoreactivity in a $CAII^+$ cluster. **(C)** PDE2A immunoreactivity in the same section as (B). **(D)** Overlay of (B) and (C). **(E)** A coronal section of the caudal OB showing $CAII^+$ glomeruli (arrows) with largely bilateral symmetry. **(F)** High-power view of CAII immunoreactivity within the dashed box in **(E)**. **(G)** PDE2A immunoreactivity. **(H)** Overlay of (F) and (G). Blue, DAPI labeling. **(I** to **K)** CAII expression overlaps with GFP labeling in the OE of GCD-ITG mice. (I) CAII immunoreactivity. (J) GFP immunoreactivity within the same region as (I). (K) Overlay of (I) and (J). **(L** to **N)** CAII expression overlaps with GFP labeling in the OB of GCD-ITG mice. (L) $CAII^+$ glomeruli. (M) GFP^+ glomeruli within the same region as (L). (N) Overlay of (L) and (M). Scale bars in (B), 20 μm; (F), 100 μm; (I), 10 μm; and (L), 50 μm.

[1]National Institute of Biological Sciences, Beijing, 102206, China. [2]Institute of Biophysics, Chinese Academy of Sciences, Beijing, 100101, China. [3]Department of Molecular Genetics and Microbiology, Duke University Medical Center, Durham, NC 27710, USA. [4]The Rockefeller University, 1230 York Avenue, New York, NY 10021, USA.

*These authors contributed equally to this work.
†To whom correspondence should be addressed. E-mail: luominmin@nibs.ac.cn

To test CO_2 sensitivity in vivo, we recorded from bulbar neurons associated with the necklace glomeruli after exposing anesthetized mice to CO_2 in the airflow delivered to their nostrils (*18*). Out of ~5000 cells tested with 0.5% CO_2 in the gas phase, excitatory responses were found in 260 cells, almost all of which were near the necklace glomeruli. By juxtacellular labeling, we identified five cells with dendritic processes that were delineated clearly and extended into the necklace glomeruli (Fig. 3A). These five cells were activated by external CO_2 at levels above 0.1% (Fig. 3, B and D). Excitatory responses to CO_2 pulses were characterized by initial bursting with short latency [306.3 ± 22.6 ms (mean ± SEM, n = 24 cells)], vigorous firing throughout the stimulus, and brief inhibition after stimulus termination (Fig. 3C). Control pulses (0% CO_2 and 20% O_2) with the same flow rate had no effect, confirming that the responses were evoked by CO_2 but not by increased airflow. The CO_2 responses of bulbar neurons were dose-dependent (Fig. 3, D and E). For the 18 most sensitive cells tested with a range of concentrations, significant activation was observed at 0.1% CO_2. Response amplitudes rose steeply between 0.1 and 0.3% CO_2 and saturated near 0.5% (Fig. 3E). Lower sensitivity to CO_2 was observed in some neurons, with saturation above 2% (n = 30 cells). Activation of GC-D$^+$ glomeruli by CO_2 was further confirmed by immunostaining against c-Fos, a marker of neuronal activation in the olfactory bulb (*17*) (fig. S5).

Finally, we used behavioral assays to examine the sensitivity of CO_2 detection by the mouse (*18*). Water-deprived adult mice were trained to lick a port for water delivery during 0.5% CO_2 pulses and to not lick during control pulses with the same flow rate and oxygen concentrations (fig. S6) (*18*). Training over ~10 days resulted in stable performance at levels of >90% correct responses (Fig. 4A, n =10 mice). During tests, response accuracy remained high for test stimuli with ≥0.1% CO_2 but fell sharply to near-chance level as CO_2 levels decreased further (Fig. 4B). The response ratio at different CO_2 concentrations fitted to a Weibull psychometric function reporting a CO_2 detection threshold of –1.18 ± 0.07 log units or 0.066% CO_2 (Fig. 4B and fig. S7, n = 8 mice) (*24*), which is just above the average CO_2 concentration in the atmosphere. The behavioral threshold also matched the response sensitivity of bulbar neurons (Fig. 3E). When the OE was ablated by nasal irrigation with zinc sulfate (50 µl at a concentration of 5%), mice were unable to detect 0.5% CO_2 pulses (Fig. 4C). Consistent with OSN regeneration, they slowly regained their ability in 1 to 2 weeks (*25*).

CO_2 repels *Drosophila* (*4*) but attracts mosquitoes to hosts (*3*). In a T-maze assay, we found that mice avoided CO_2 at concentrations as low as 0.2% (n = 31 mice, $P < 0.01$, t test). The avoidance became substantially more marked at higher concentrations (Fig. 4D, 0.4 to 3.2% CO_2). Lesions of the OE by nasal irrigation with zinc sulfate eliminated the avoidance of CO_2 (Fig. 4D). The effects of lesions on mice both trained and untrained for CO_2 detection, in combination with the fast reaction time for CO_2 detection (fig. S8) and the low CO_2 sensitivity of the trigeminal system (fig. S9), demonstrate that the OE has a direct role in CO_2 detection.

Because CAII is expressed exclusively in GC-D$^+$ neurons and its activity is essential for CO_2 responses in these neurons (Figs. 1 and 2), we examined the behavioral phenotype of mice homozygous for a null mutation in the *CAII/Car2* gene that was induced by chemical mutagenesis with *N*-ethyl-*N*-nitrosourea (fig. S10) (*20*, *26*). These mutant mice were unable to detect CO_2 at concentrations below 1% (fig. S11), but their learning curve and detection threshold for detecting amyl acetate (0.10% saturated vapor) were indistinguishable from those of wild-type mice (Fig. 4E, n = 6 for mutant and 7 for wild-type mice) (*18*). After learning the behavioral paradigm with amyl acetate, both wild-type and *CAII*

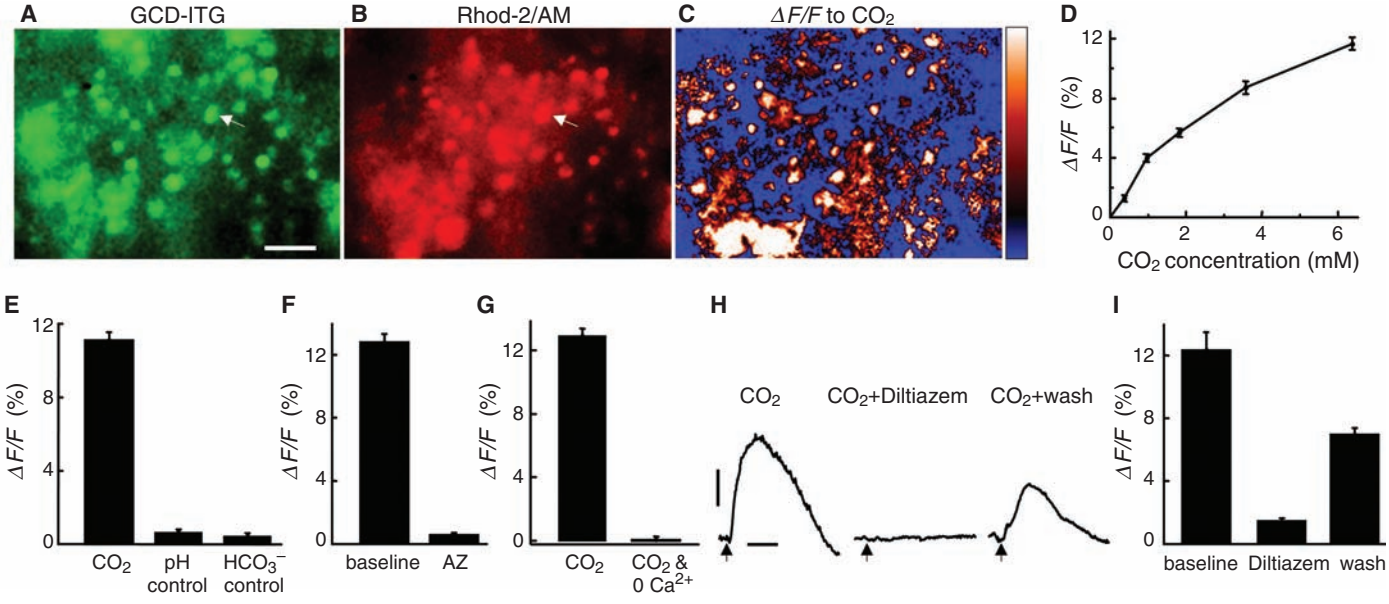

Fig. 2. CO_2 activates GC-D$^+$ neurons, and this activation requires CA activity and the opening of CNG channels. (**A**) GFP labeling of a cluster of GC-D$^+$ neurons within an intact epithelial preparation from a GCD-ITG mouse. The arrow points to a dendritic knob. (**B**) Uptake of the calcium-sensitive dye rhod-2 AM into GC-D$^+$ neurons within the same region as (A). (**C**) Map of normalized fluorescence changes ($\Delta F/F$) within the same region as (A) and (B) showing activation of GC-D$^+$ neurons after CO_2 application. The color scale at the right indicates a $\Delta F/F$ range of 0 to 20%. For all GC-D$^+$ neurons tested, $\Delta F/F$ = 11.1 ± 0.4% (mean ± SEM, n = 428 cells, 8 mice). (**D**) Dose-response curve of the calcium signal to CO_2 (n = 123 cells). (**E**) Group data showing that GC-D$^+$ neurons respond to 6.4 mM CO_2 but not to pH-adjusted and bicarbonate controls ($\Delta F/F$ = 0.7 ± 0.1% for pH-adjusted control, n = 123 neurons, $P < 0.001$, t test, CO_2 versus pH-adjusted control; $\Delta F/F$ = 0.4 ± 0.2% for bicarbonate control, n = 170 neurons, $P < 0.001$, t test, CO_2 versus bicarbonate). Error bars in this and the following figures indicate SEM. (**F**) Group data showing blockade of CO_2 responses by the CA inhibitor AZ ($\Delta F/F$ = 12.8 ± 0.5% in baseline conditions versus 0.5 ± 0.1% in AZ, n = 225 neurons, $P < 0.001$, t test). (**G**) Group data showing the absence of CO_2 responses in Ca^{2+}-free Ringer solution ($\Delta F/F$ = 13.0 ± 0.5% in normal Ringer solution versus 0.0 ± 0.1% for Ca^{2+}-free Ringer, n = 118 neurons, $P < 0.001$, t test). (**H** and **I**) A single example (H) and group data (I) showing the reversible blockade of CO_2 responses by L-*cis*-diltiazem ($\Delta F/F$ = 12.3 ± 1.1% in baseline, 1.8 ± 0.3% during diltiazem application, and 6.9 ± 0.5% during washout; n = 225; $P < 0.001$; t test). Scale bar in (A), 10 µm; in (H), 50 s and a $\Delta F/F$ of 10%.

mutant mice learned to switch to acetophenone as the new rewarding stimulus (Fig. 4E). Whereas wild-type mice switched to CO_2 as the new rewarding stimulus in less than 50 trials, *CAII* mutant mice could not do so even after intensive training (Fig. 4E). Thus, *CAII* mutant mice have profound deficits in detecting CO_2 but not other odorants. To confirm whether CA in the OE is critical for the sensitive detection of CO_2, we applied the CA inhibitor AZ (50 μl at a concentration of 15%) to the nasal cavities of trained wild-type mice. The application of AZ but not of saline reversibly abolished the animals' ability to detect CO_2 but not amyl acetate (fig. S12). Conventional OSNs require CNG channels consisting of CNGA2 subunits for odorant detection, and *CNGA2* knockout mice are profoundly compromised in their sense of smell (*17*, *27*). However, *CNGA2* mutant mice had apparently normal CO_2 learning curves and detection thresholds (fig. S13, $n = 4$ mice). Together, these results demonstrate that sensitive CO_2 detection is exclusively mediated by GC-D^+ neurons.

In this study, we identify the GC-D^+ neurons as the olfactory subsystem that mediates CO_2 detection in mice. It remains possible that GC-D^+ neurons can detect other chemicals. CO_2 responses in the GC-D^+ neurons require CA enzymatic activity and the opening of CNG channels. We hypothesize that CAII converts CO_2, a highly diffusible gas, into intracellular HCO_3^- and H^+, and that these ions in turn enhance cGMP levels and trigger the opening of CNG channels in GC-D^+ neurons. The CO_2-responsive neurons in insects provide a model system for studying innate behavior linked to a small number of neurons (*4*, *6*). Similarly, GC-D^+ neurons may be used as a model system for investigating innate avoidance behavior in mammals. Mammals have adapted to low-CO_2 environments (~0.03%) for millions of years (*28*). Some studies predict that the global CO_2 level will exceed the detection threshold for mice within one century (*29*). Rising atmospheric CO_2 levels may have ecological and ethological impacts on mammalian behavior.

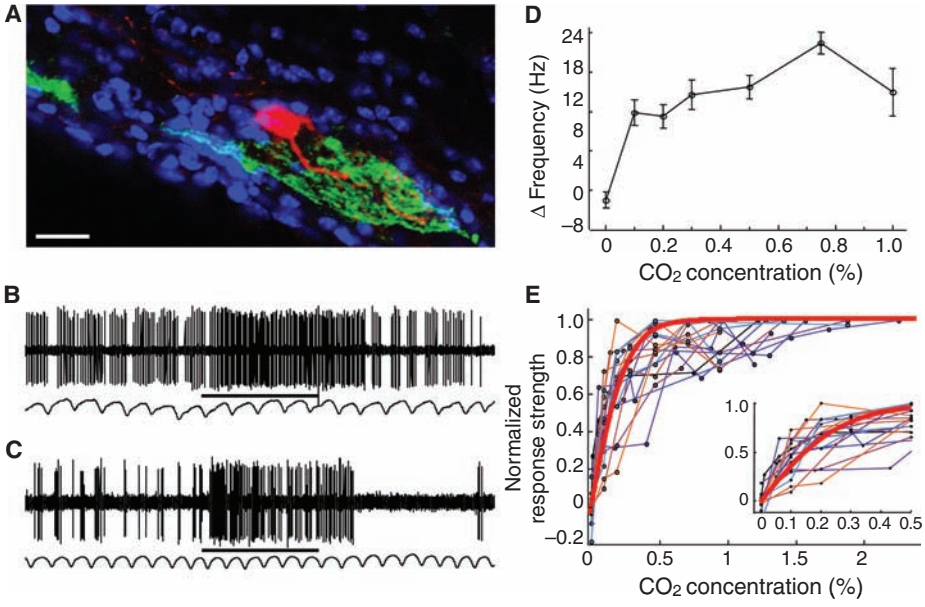

Fig. 3. CO_2 response pattern and CO_2 sensitivity of bulbar neurons in vivo evoked by exposing mice to CO_2 in the airflow delivered to the nostrils. **(A)** Morphology of a cell with dendrites (red) extending into a $CAII^+$ glomerulus (green). DAPI labeling (blue) delineates glomeruli. **(B)** Physiological trace of the cell in (A) showing vigorous response to 0.5% CO_2. Horizontal bar at bottom indicates a 2-s CO_2 pulse. The bottom trace indicates the respiratory rhythm monitored simultaneously. **(C)** Response pattern of another bulbar cell to a 0.5% CO_2 pulse. **(D)** Dose-response curve of the cell in (A). **(E)** Dose-response curves of the 18 most sensitive neurons (connected lines of different colors). The thick red curve represents fitting with a sigmoid function. The inset shows a zoomed view between 0 and 0.5% CO_2. Significant responses were observed at 0.1% CO_2 (46.0 ± 0.5% of maximum responses, $P < 0.001$ compared to baseline, *t* test). Scale bar in (A), 20 μm.

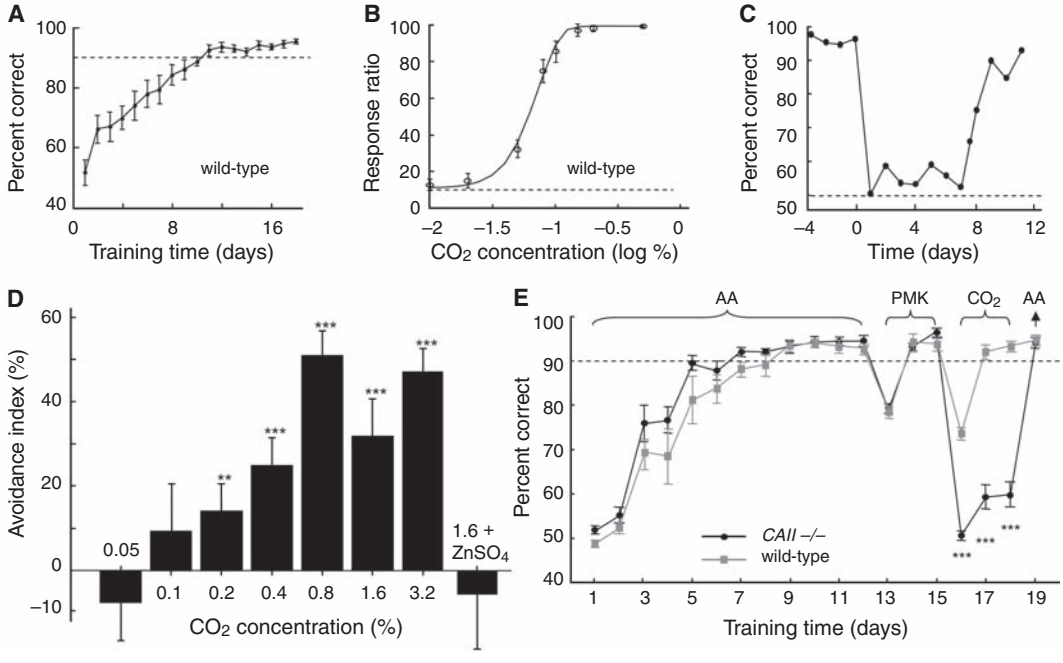

Fig. 4. Mice detect CO_2 with behavioral thresholds near atmospheric levels. **(A)** Learning curve for CO_2 detection by wild-type mice. The dashed line indicates 90% correct. **(B)** Mean response ratio to different CO_2 concentrations from test sessions over 7 days. The curve indicates data fitting with a Weibull psychometric function. The dashed line indicates near-chance response level to 0% CO_2. **(C)** After lesion of the OE with 5% zinc sulfate (day 0), the mouse's ability to detect 0.5% CO_2 was eliminated over the following day (percent correct = 46.2 ± 4.1%, $n = 5$ mice, $P < 0.001$; within group *t* test) and then gradually recovered within 7 to 14 days. **(D)** CO_2 leads to avoidance behavior. Bars indicate the avoidance index revealed by T-maze tests. Avoidance of CO_2 was abolished by lesions of the OE after nasal irrigation with 5% zinc sulfate. $^{**}P < 0.01$; $^{***}P < 0.001$, *t* test. **(E)** Learning curves of both wild-type (gray line and squares) and CAII mutant mice (black line and circles) for odorant and 0.5% CO_2 detection. AA, amyl acetate; PMK, phenylmethylketone, also known as acetophenone. $^{***}P < 0.001$ for comparison between wild-type and mutant mice.

References and Notes

1. G. Stange, S. Stowe, *Microsc. Res. Tech.* **47**, 416 (1999).
2. S. Lahiri, R. E. Forster 2nd, *Int. J. Biochem. Cell Biol.* **35**, 1413 (2003).
3. M. T. Gillies, *Bull. Entomol. Res.* **70**, 525 (1980).
4. G. S. Suh *et al.*, *Nature* **431**, 854 (2004).
5. C. Thom, P. G. Guerenstein, W. L. Mechaber, J. G. Hildebrand, *J. Chem. Ecol.* **30**, 1285 (2004).
6. W. D. Jones, P. Cayirlioglu, I. G. Kadow, L. B. Vosshall, *Nature* **445**, 86 (2007).
7. D. Shusterman, P. C. Avila, *Chem. Senses* **28**, 595 (2003).
8. E. L. Coates, *Respir. Physiol.* **129**, 219 (2001).
9. M. Kimoto *et al.*, *J. Histochem. Cytochem.* **52**, 1057 (2004).
10. S. L. Youngentob, D. E. Hornung, M. M. Mozell, *Physiol. Behav.* **49**, 21 (1991).
11. K. E. Ferris, R. D. Clark, E. L. Coates, *Chem. Senses* **32**, 263 (2007).
12. H. J. Fulle *et al.*, *Proc. Natl. Acad. Sci. U.S.A.* **92**, 3571 (1995).
13. D. M. Juilfs *et al.*, *Proc. Natl. Acad. Sci. U.S.A.* **94**, 3388 (1997).
14. M. R. Meyer, A. Angele, E. Kremmer, U. B. Kaupp, F. Muller, *Proc. Natl. Acad. Sci. U.S.A.* **97**, 10595 (2000).
15. K. Shinoda, T. Ohtsuki, M. Nagano, T. Okumura, *Brain Res.* **618**, 160 (1993).
16. M. H. Teicher, W. B. Stewart, J. S. Kauer, G. M. Shepherd, *Brain Res.* **194**, 530 (1980).
17. W. Lin, J. Arellano, B. Slotnick, D. Restrepo, *J. Neurosci.* **24**, 3703 (2004).
18. Materials and methods are available as supporting material on *Science* Online.
19. R. G. Khalifah, *J. Biol. Chem.* **246**, 2561 (1971).
20. P. Pan *et al.*, *J. Physiol.* **571**, 319 (2006).
21. M. Ma, G. M. Shepherd, *Proc. Natl. Acad. Sci. U.S.A.* **97**, 12869 (2000).
22. H. Harned, R. J. Davis, *J. Am. Chem. Soc.* **65**, 2030 (1943).
23. T. Y. Chen *et al.*, *Nature* **362**, 764 (1993).
24. A. C. Clevenger, D. Restrepo, *Chem. Senses* **31**, 9 (2006).
25. K. McBride, B. Slotnick, F. L. Margolis, *Chem. Senses* **28**, 659 (2003).
26. S. E. Lewis, R. P. Erickson, L. B. Barnett, P. J. Venta, R. E. Tashian, *Proc. Natl. Acad. Sci. U.S.A.* **85**, 1962 (1988).
27. L. J. Brunet, G. H. Gold, J. Ngai, *Neuron* **17**, 681 (1996).
28. P. N. Pearson, M. R. Palmer, *Nature* **406**, 695 (2000).
29. P. M. Cox, R. A. Betts, C. D. Jones, S. A. Spall, I. J. Totterdell, *Nature* **408**, 184 (2000).

30. We dedicate this paper to the memory of L. C. Katz. We thank H. Zhao for *CNGA2*-knockout mice; J. A. Beavo for antibodies against PDE2A; C. Zhan, Y. Lu, and M. Kubota for technical assistance; M. Ma for technical advice; and A. Person, P. Sterling, and R. Roberts for comments on the manuscript. M.L. is supported by the China Ministry of Science and Technology, a Natural Science Foundation of China Young-Investigator Grant, and a Human Frontier Science Program grant jointly to H.M. and M.L. Support from NIH grants went to H.M., A.W., and P.M. Questions about GCD-ITG mice should be addressed to P.M. (peter@rockefeller.edu).

Supporting Online Material

www.sciencemag.org/cgi/content/full/317/5840/953/DC1
Materials and Methods
Figs. S1 to S13
References

25 April 2007; accepted 12 July 2007
10.1126/science.1144233

Structure of the Membrane Protein FhaC: A Member of the Omp85-TpsB Transporter Superfamily

Bernard Clantin,[1,2,3] Anne-Sophie Delattre,[2,3,4] Prakash Rucktooa,[1,2,3] Nathalie Saint,[5,6] Albano C. Méli,[5,6] Camille Locht,[2,3,4] Françoise Jacob-Dubuisson,[2,3,4]* Vincent Villeret[1,2,3]*

In Gram-negative bacteria and eukaryotic organelles, β-barrel proteins of the outer membrane protein 85–two-partner secretion B (Omp85-TpsB) superfamily are essential components of protein transport machineries. The TpsB transporter FhaC mediates the secretion of *Bordetella pertussis* filamentous hemagglutinin (FHA). We report the 3.15 Å crystal structure of FhaC. The transporter comprises a 16-stranded β barrel that is occluded by an N-terminal α helix and an extracellular loop and a periplasmic module composed of two aligned polypeptide-transport–associated (POTRA) domains. Functional data reveal that FHA binds to the POTRA 1 domain via its N-terminal domain and likely translocates the adhesin-repeated motifs in an extended hairpin conformation, with folding occurring at the cell surface. General features of the mechanism obtained here are likely to apply throughout the superfamily.

Targeting of proteins to their dedicated subcellular compartments is essential for cell function and organelle biogenesis. Translocation of proteins across or insertion into membranes is mediated by protein machineries, some of which have been conserved throughout evolution, such as the transporters of the Omp85-TpsB superfamily. TpsB transporters are components of two-partner secretion (TPS) systems in Gram-negative bacteria. They secrete large, mostly β-helical proteins called TpsA proteins that generally serve as virulence factors (*1*, *2*). TpsB transporters function without accessory factors. The superfamily also includes the Toc75, Sam50-Tob55, and Omp85-YaeT homologs, which are the cores of large hetero-oligomeric complexes involved in protein transport across, and insertion of β-barrel proteins into, the outer membranes of chloroplasts, mitochondria, and Gram-negative bacteria, respectively (*3*–*9*).

Omp85-TpsB transporters have been predicted to comprise a conserved C-terminal transmembrane β barrel and a soluble N-terminal region harboring one to five putative polypeptide-transport-associated (POTRA) domains, which are hypothesized to mediate protein-protein interactions (*10*–*12*). The transporters also harbor conserved C-proximal signature motifs of unknown function in their pore-forming regions (*13*). In spite of their implication in critical physiological processes such as membrane biogenesis and secretion of virulence proteins, the molecular mechanisms of protein translocation or insertion into membranes by those transporters remain poorly understood. To address these issues, we determined the crystal structure of the TpsB prototype FhaC that mediates the translocation to the bacterial surface of filamentous hemagglutinin (FHA), the major adhesin of the whooping cough agent *Bordetella pertussis*.

FhaC was crystallized in space group $C222_1$, and the crystals contained one molecule in the asymmetric unit. The structure was solved by the single-wavelength anomalous diffusion (SAD) method (*14*) and is reported to a resolution of 3.15 Å (table S1 and fig. S1). The protein is a monomer and comprises a 35 Å high β barrel composed of 16 antiparallel β strands (B1 to B16) (Fig. 1A and fig. S2) with a shear number of 20. The β barrel corresponds to the C-terminal moiety of the protein and encompasses residues 209 to 554. The periplasmic and extracellular sides of the barrel are characterized by short turns and longer loops (L1 to L8), respectively, in general agreement with a prior topology model (*15*). The N terminus of the protein is located in the extracellular milieu and folds into a 20-residue-long α helix (H1) that goes right through the transmembrane β barrel (Fig. 1, A and B). The C terminus of helix H1 emerges into the periplasm and is connected to a periplasmic module via a 30–amino acids linker that has no well-defined electron density in the crystal structure. This periplasmic module of 150 residues precedes the β barrel, a feature that had not been predicted earlier (*15*).

The interior of the β barrel is partly hydrophilic, with 17 charged residues pointing inward. Helix H1 is also charged with six Lys and/or Arg and six Asp and/or Glu residues. The charged residues are not uniformly distributed inside the barrel but form three clusters (fig. S3). Cluster 1 runs from the periplasm to the bacterial surface and comprises residues Arg^{280} and Asp^{282} (B5), Lys^{313} (B6), Lys^{333} and Arg^{335} (B7), Asp^{355} (B8), and

[1]UMR8161 CNRS, Institut de Biologie de Lille, Université de Lille 1, Université de Lille 2, 1 rue du Prof. Calmette, F-59021 Lille cedex, France. [2]Institut Pasteur de Lille, Lille, 1 rue du Prof. Calmette, F-59019 Lille cedex, France. [3]IFR142, 59019 Lille, France. [4]INSERM, U629, 59019 Lille, France. [5]INSERM, U554, 34090 Montpellier, France. [6]UMR5048 CNRS, Université de Montpellier 1, Université de Montpellier 2, Montpellier, France.

*To whom correspondence should be addressed. E-mail: francoise.jacob@ibl.fr (F.J.-D.); vincent.villeret@ibl.fr (V.V.)